Paper presented at the 65th International Astronautical Congress 2014: Our World Needs Space (IAC)
Toronto, ON, Canada, Sept. 29-Oct. 3, 2014

IAC-14-A6.5.2

DEPLOYABLE MECHANISMS FOR SMALL TO MEDIUM SIZED SPACE DEBRIS REMOVAL

David St-Onge
Laval University, david.st-onge.2@ulaval.ca
Clément Gosselin
Laval University, gosselin@gmc.ulaval.ca

Abstract

This research aims to propose a new paradigm in orbital debris removal systems. While most groups addressing this issue focus on the high priority of removing the largest debris, we consider the threat posed by those smaller than 10cm as serious. A 2cm paint chip is known to be able to render useless most spacecraft as well as being way more difficult to follow and thus to avoid. We propose a mission to sweep the main Low Earth Orbits with a 100 to 500 metre diameter cupola that would collect small debris. The cupola consists of a deployable mechanism supporting a membrane. The deployment mechanism has to reach a minimal expansion ratio of about 30, in order to create a very wide collecting surface. The membrane covering its surface would be rigid enough to capture most small debris and to at least slow down the medium-sized ones, accelerating their fall. An overview of our almost-rigid-link mechanism proposed to support the collecting surface is presented. The proposed mechanisms is based on previous work on deployable mechanisms developed for a variety of applications. However, conventional deployable rigid-link mechanisms typically produce expansions that are much smaller that the ratio required in the present application. Therefore, cable or belts systems are included in order to further increase the expansion ratio while maintaining a low mass. While in operation, the cupola will obviously be subjected to many ultra-high-velocity impacts and its orientation will likely undergo deviations from the targeted optimum. Therefore, another important feature of the proposed debris removal concept is the development of means of reorienting and stabilizing the cupola using internal electric deployment actuators instead of fuel thrusters. The concept of reorientation using internal actuators is presented and simple examples are provided. Finally, the performance of the concept is confronted to data analysis from MASTER09 and with the recent release of ORDEM3. This data serves as the basis for the design specifications. Space debris removal is a high priority for the future of space missions and space exploration. The approach proposed here is believed to be one of the pieces of the puzzle.

1 INTRODUCTION

Awareness of the threat posed by space debris has been growing in the scientific community for more than a decade and more recently in the general population[1]. Research groups are focusing on retrieving the large debris, easily tractable and posing a threat to future space missions. Unfortunately smaller size debris is not that simple to track and thus to retrieve or even to avoid with spacecraft maneuvers. Lately a note from J-C Liou in the NASA Orbital Debris journal states that in order to reduce mission-ending threats to operational spacecraft, the focus should be to remove the 5mm to 1cm debris[1]. The problem of grasping or slowing down large debris was adressed intensively in the past decade, but small and medium sized debris removal requires an area-time product of thousands of $km^2.year$ to be meaningful. In other words, the larger the device to sweep the orbit volume, the shorter the mission time to retrieve a given amount of space debris.

[1] *Gravity* movie shown in 3820 theaters, Warner Bros. Pictures, 2013.

With available rocket payloads, the first step is to pack a large device (0.5km) in a relatively restricted space (10m). Deployable systems are being studied for telescopes, sails and solar panels in space [2], but existing solutions are either too fragile to resist many small hits (as with inflatable membranes) or too small at full extension.

We introduce a belt-driven rigid planar mechanism with a high expansion ratio taking advantage of both robust rigid links and light belt driving transmission. The triangular mechanism is meant to be a base unit to assemble any surface which can be tessallated. Such a large surface will be subjected to torque reaction from the debris hits and thus will need frequent re-orientation. Instead of using common costly fuel thrusters we present here a new internal actuator concept to control the orientation of the device without the needs for dedicated actuators and fuel. To understand the context and requirements of this design we first present the small to medium sized debris population and our targets.

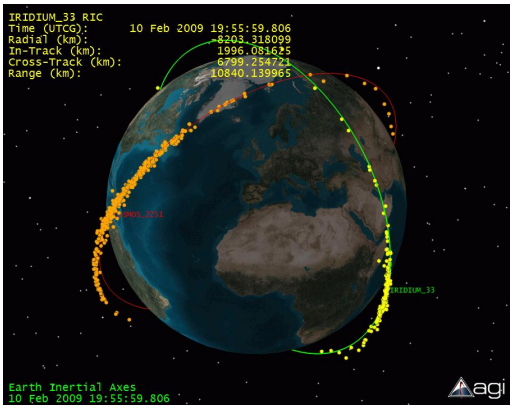

Figure 1: Debris cloud after the Iridium/Cosmos collision (Celestrak/AGI Viewer 9)

2 MISSION PARAMETERS

2.1 LEO debris model

In 1978, Dr. Kessler and Dr. Cour-Palais developed a model predicting that the orbital debris population will reach a point where it will inevitably grow exponentially in an uncontrollable chain reaction [3]. The number of debris will be so important that impacts will not be preventable; dispersing, multiplying their number and preventing any spacecraft to be safely launched, reaching a point where each new spacecraft will be hit by some space debris, adding itself to the list of drifting objects. It is possible that the situation has already passed the no-return point, mainly since the 2007 and 2009 collisions [4]. The latter involved a commercial satellite, Iridium-33 (560kg)[2] and the military Russian satellite Cosmos-2251 (900kg), out of service for 10 years [5], creating thousand of new small-to-medium sized debris as shown in figure 1.

Even in a scenario in which we would stop launching new spacecraft, objects already on orbit will collide with one another until their number prevents any further space mission without high risk. Since year 2000, the National Centre for Spatial Studies in France[3] has been monitoring the debris population and has been working on predicting their evolution as well as ways to retrieve them [4]. Following one of their studies, a satellite already on orbit has from 3% to 5% chances to lose functionality because of a debris impact within the next 7 years of operation.

The most crowded orbits in terms of debris are the ones popular for Earth observation and satellite-based communications, called the Low Earth Orbits, below 2000km of altitude. On these orbits, debris as small as 1mm can be statistically tracked (interpolation of returning spacecraft shielding and atmosphere density). The large debris are getting most attention because one percent of all debris represents 99% of the overall mass to be removed from space [6]. Large debris also have the potential to generate a lot more debris if they collide. By removing 5 of these per year, the growing rate of debris will stop (over 200 years) and the number of collisions over the same period would drop from 45 to 27 [7].

But the number of the remaining 99%, mostly debris smaller than 10cm, was determined to be over 170 billions in July 2013[4]. If the American parts of the International Space Station (ISS) are made to resist impact of objects under 1.4cm, this is not the case for all spacecraft. In 2012, about 1200 objects of more than 1.5cm crossed the path of the ISS, from which 800 were under 3cm. A collector of $1000 km^2.an$ would be required to cut by half this quantity [8]. Depending on the component destroyed by a debris collision, the consequences vary. These small debris impacts are better understood thanks to scientific installations on the space stations (Mir, ISS and Skylab) as well as the inspection of returning spacecraft [9, 10, 11, 12].

An object as small as a paint chip, common in orbit, can render useless a satellite. The speed at which LEO objects are moving is computed by equating the centrifugal

[2] part of the telecommunication satellite constellation Iridium
[3] CNES
[4] from ESA website, last visited on 09/09/2014

and gravitational forces:

$$F_G = \frac{Gm_E m_S}{r^2} \text{ and } F_C = \frac{m_S v^2}{r} \text{ , hence } v = \sqrt{\frac{Gm_E}{R_O + R_E}} \quad (1)$$

For orbital distance (R_O) of 300km to 2000km we then get:

$$v = \sqrt{\frac{(6,673x10^{-11}\frac{Nm}{kg})(5,974x10^{24}kg)}{R_O + 6378km}} = [6,6-7,4]\frac{km}{s} \quad (2)$$

Hence, the absolute relative speed between 2 objects in LEO will be between 0 to 15km/s. Hence, a small paint chip (approximated by an aluminum sphere of 2.44g) can transfer an energy of 56kJ by hypervelocity impact. At these hypervelocities, an object of about 25g has the same momentum as a 1360kg car driving at 100km/h [13].

Apart from the dynamics of impact at hypervelocity, a complex aspect is their traveling dynamics: their high area-to-mass ratio makes them vulnerable to atmospheric perturbations. The populations below 1000km have strong short-term variations (monthly). Debris smaller than 10cm are expected to re-enter the atmosphere slightly more rapidly, but their substantially greater numbers results in even greater collision risks to operational spacecraft in LEO [14].

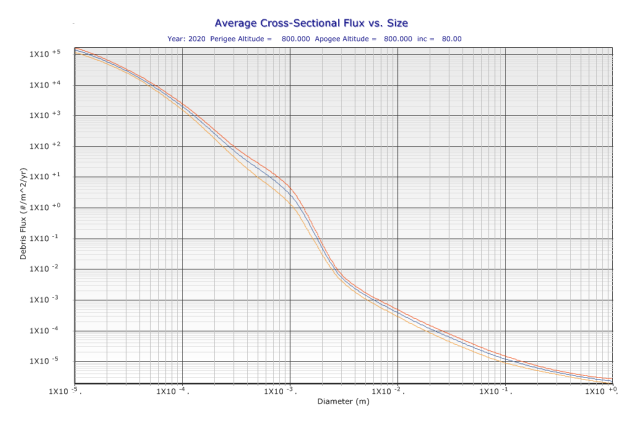

Figure 2: Projected debris flux according to size at 800km altitude, 80˚declination in 2020 (ORDEM3)

Since most data analysis focus on large debris we search for the specific flux of the small-to-medium sized ones using ORDEM3.0. This software developed and shared by NASA gives a quick and up-to-date overview of the situation. We observe from figure 2 that the majority of the flux comes from debris smaller then 1cm. We can also state that at 800km altitude a little more than 200 objects over 5cm in size may hit a 0.5km device over a year. The analysis is restricted to objects between 1cm to 10cm, since below that range most shielding can withstand an impact and above that other strategies must be applied. Within this range, there is approximately 670000 objects on all Earth orbits.

2.2 Mission objectives

Three main parameters influence the mission planing: the area swept, the time spent on orbit and the target orbit (altitude and declination). All three are correlated to the number of objects retrieved. From the MASTER09 simulation in figure 3, the most populated orbits are around 800km to 1000km altitude and 80˚ to 100˚ declination. Selecting one of the most crowded orbits as the target, say 800km altitude and 80˚ declination, the other two parameters are shown in figure 4.

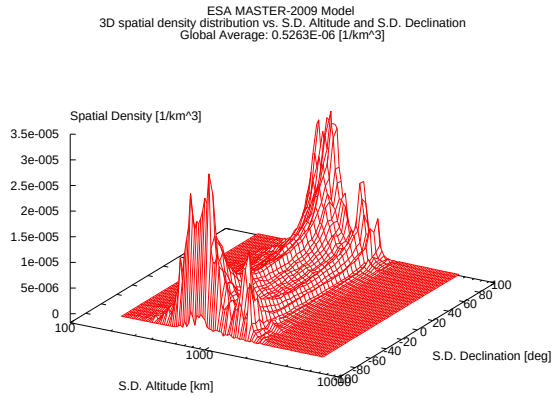

Figure 3: Density of small-to-medium sized debris on LEO (MASTER09)

From the latter, a disk of 250m radius will catch or slow down over 1900 objects between 1cm and 10cm while on orbit for a year and possibly a lot more of smaller size. Considering an approximated weight of 9450kg (30 units of 115kg[5] structure and 200kg membrane[6]) and a cost of 3600$ per kilogram [16], the price per piece of debris touched is growing quickly with the time spent on orbit (1200$/debris for a single year).

The physical dimensions of the system need to fit a standard launching platform. The selected rocket is the commercial Ariane 5, operated by Airbus Defense [17]. It can contain 10000kg of material and potentially 2 satellites as

[5] Considering full aluminium structure

[6] Assuming a "membrane" made of silicone ($968kg/m^3$), such as the widely used space grade encapsulant DC-93-500[15], with 20% kevlar fibers ($1400kg/m^3$), to form 50m side triangular unit (extended) of $175\mu m$ (standard thickness of a solar array back panel protector [10])

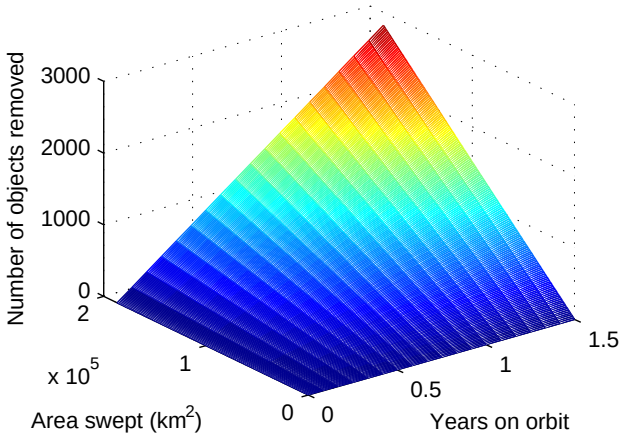

Figure 4: Number of objects (1cm to 10cm) collected versus area and year on orbit in 2020 (ORDEM3)

shown in figure 5. It is possible to use the whole large cargo space or to split the cost by launching 2 missions together.

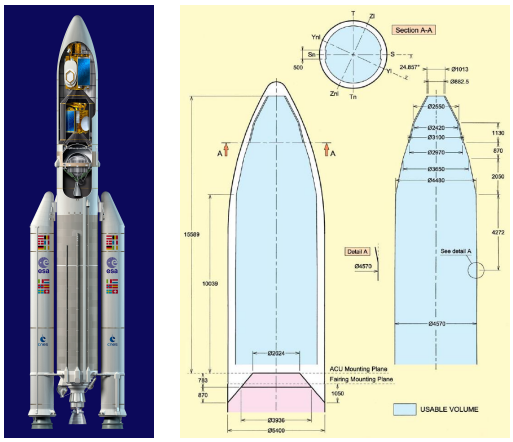

Figure 5: ESA Ariane 5 [17]

The payload space is a cylinder of approximately 4.5m diameter by 10m height.

The membrane is not expected to resist an impact with a small object at opposite velocity – approximately 15km/s relative velocity – but it should rip on impact without creating more debris and thus slowing it down. The membrane design is not covered by this study but a promising material configuration could be the stuffed Whipple shield, making use of flexible layers of Kevlar and Nextek fabrics.

3 MECHANISM

3.1 1 Dof rigid-link planar mechanism

A wide variety of deployable mechanisms were proposed for space applications where the dimensions at launch are limited [2, 18]. Some of these mechanisms are being used currently mainly for telescopes or telecomunication cupolas and solar panels. Solar sails can also benefit from deployable mechanisms since the area required to produce a relevant thrust is considerable. De-orbiting and re-entry devices are now adding to the list, since the IADC debris mitigation report [19] states that it is essential to such feature before launch, but still the avaible space and payload are extremely limited. The solution may reside in inflatable or deployable mechanisms. The University of Naples already suggested devices for the CubeSat and the NanoSat [20]. Recent mission projects for Mars and Moon based stations renew interest in inflatable structures. If the latter require more research to stabilize (or rigidize) their shape after inflation, most of these mechanisms are unstable and hard to control in the deployment phase. Extending masts may get stuck or thin folded membranes ripped. We aim to find a robust and rigid solution.

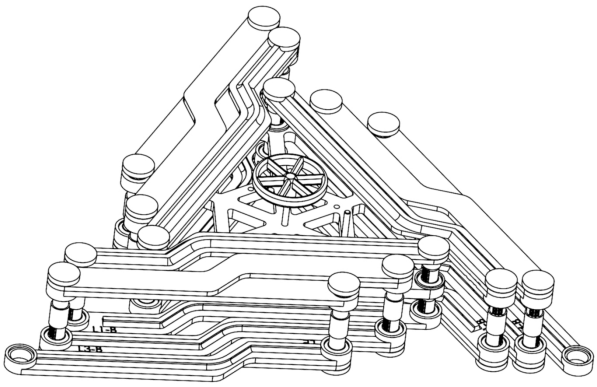

Figure 6: Belt-driven module

Based on previous work on expandable one-degree-of-freedom three-dimensional structures [21], inspired by the work of Wohlhart [22] and the results presented by Wei [23], we introduce a new almost-rigid-link deployable planar mechanism. Instead of using linkages to extend each section of each leg in the mechanism to ensure symmetrical deployment from the only actuator, it uses timing belts. The design and specificities of the belt-driven mechanism are the subject of a separate publication [24], but we will quickly explain its geometry and introduce an optimization

for the context of this paper.

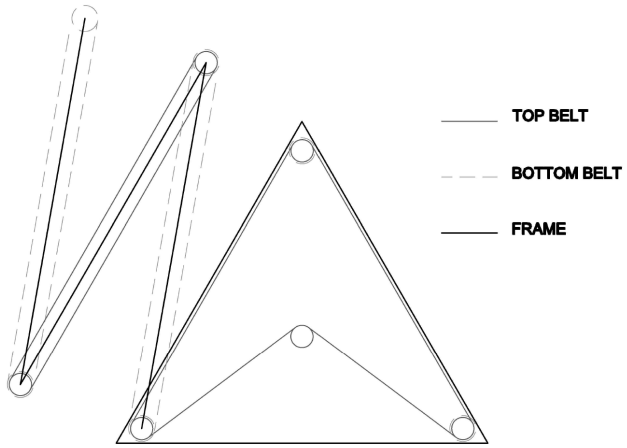

Figure 7: Belt-driven mechanism schematic

The pulleys and the respective joints share the same axis, yet, they can freely rotate around it without transmitting the rotation to the link. Each member has a fixed pulley on each end, and the driving belts join two non adjacent members. For instance, member 1 drives member 3 (through a top belt in figure 7), while member 2 and 1 are driven by the base (respectively by a bottom and top belt in figure 7), thus the mechanism has only one degree of freedom. The design is hard to parameterize due to assembly constraints referred to as the *virtual triangle* [24], but is approximated in this context to allow a basic optimization. The ratio is obtained from the deployed height of a triangular face, H_D, to its retracted height, H_R:

$$R_P = \frac{H_D}{H_R} \tag{3}$$

Both of these quantities depend on the number of links on each leg, the length of each of these links, their width and the height of the inner fixed triangle. Based on the rocket launcher geometry constraint, the space available for a face is a disk of 4.5 metre diameter and thus we can fix H_R to half of that and maximize H_D. From our experiment on the robustness of with plastic prototypes of this mechanism and given the possible range of link lengths (expected to be between 0.5m to 2.5m before the optimization process), the link width was uniformly set to 60mm. To further restrict the number of parameters a recursive dimensioning pattern was determined between link lengths to infer them solely from the first one. The optimization process for H_D is then defined in terms of the number of links n and the first link length l_1 as shown in figure 8.

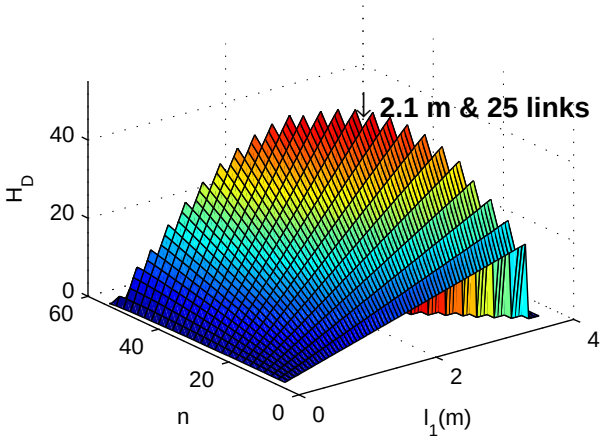

Figure 8: Optimization of extended length

The optimal configuration within this context is 25 links with the first one being 2.1m long. This design leads to a planar ratio $R_P = 23$. Based on 12mm belts, the mechanism is 75mm thick, which allows to stack a large number of units in the 10 metres long rocket cylinder (figure 10). For instance, 80 units would deploy following a folded pattern such as the one shown in figure 11 to create a final surface of $0.13km^2$.

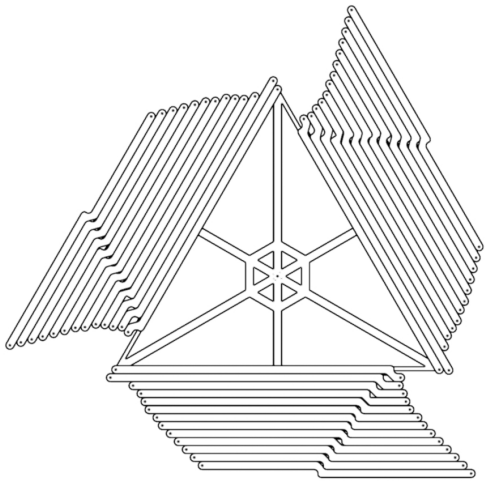

Figure 9: 25 links shuttle optimized geometry with a 2.4m side length inner triangle

The final structure has a large surface to links thickness ratio. The possible buckling of the links must also be analyzed [25]. Some structural flexibility is desirable to help

absorb the impacts of colliding debris. Compliant capture of debris was shown successful with a flexible effector and compliant joints [26].

The links were designed using a closed shape profile, enhancing their structural robustness perpendicular to the deployment direction. Since the cupola moves perpendicularly to its orbit plane, this direction is considered to be the direction of higher velocity impact. The high deployment ratio makes the surface of the links ($9.6m^2$ for a single unit) small compared to the surface of the membrane ($2815m^2$ for a single unit). Hence, any of the 200 objects over 5cm has only a probability of 0.3% of hitting the structure. For the fastest and largest ones the membrane will simply rip and the debris will be slowed down.

As shown in figures 10 and 11, the shuttle cylinder is filled with triangular faces packed one on top of the other, having only one edge physically attached to the previous and next faces. When the first phase of deployment is triggered, the spring loaded hinges between each of the adjacent faces release one after the other and the cupola is assembled in a spiral, starting from its centre. Magnetic locks on each vertex allow the shape to fully stabilize before the second deployment phase. At that point the belt mechanism on each of the faces, linked together, is controlled from the cupola centre by a single actuator. The membrane on each face unfolds itself and stretches to the fully extended surface of 415m diameter.

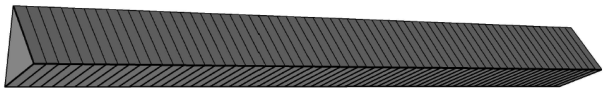

Figure 10: Folded Icocupola

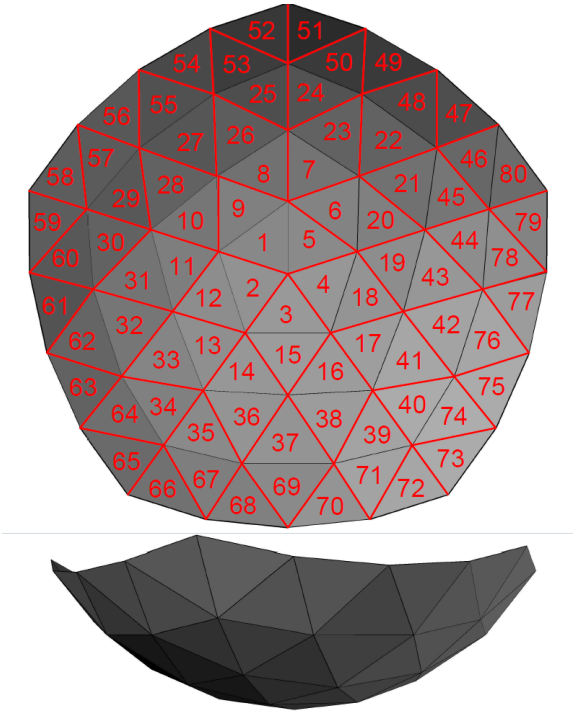

Figure 11: Folding pattern of an unfolded Icocupola

4 RE-ORIENTATION

Reorienting a spacecraft is a complex maneuver but it is required to compensate for the orbital trajectory perturbations. Many Attitude Control Systems (ACS) were developed to address this issue [27, 28, 29, 30, 31]. Free-floating space robotic systems are spacecraft manoeuvers that do not use fuel to actively control attitude - a review of the research in this area is given by Dubowsky and Papadopoulos in [32].

Our suggested approach is to control the orientation of the spacecraft using its internal actuators, thus taking advantage of a deployable mechanism or an arm to induce a moment to the free-floating object.

A free-floating rigid body without input forces and torques conserves its angular momentum, but the latter is not necessarily zero. Kolmanovsky et al. showed that with at least 4 links, a multibody system can be oriented following any trajectory whose derivative is periodic [33].

Following non-holonomic motion planning, a field of study developed around planar multibody reorientation [34, 35, 36, 37, 38, 39]. Underactuated mechanisms are a good example of such mechanisms, being nonholonomic for instance due to the constraint of a passive joint. They are popular for space applications because they reduce weight, cost and energy consumption while simplifying the structure. However, their drawbacks are the lack of redundancy and the more complex control. With the second-order nonholonomic constraint of passive joints, a rest-to-rest motion planing for a multibody planar mechanism can be achieved by controlling the planar motion of a joint $(\ddot{x}, \ddot{y}, \ddot{\theta})$ [34]. A more pratical way of actuating such mechanisms is to use only the joint actuators (as for a robot arm).

4.1 Dynamic equations

We derive the dynamic model based on two postulates:

- There is no external force to our system, so linear momentum is conserved and is zero (without loss of gen-

erality [35]):

$$\sum_{i=1}^{n} m_i \boldsymbol{v}_i = \boldsymbol{0} \tag{4}$$

- The angular momentum taken at the centre of mass of our system is conserved:

$$\sum_{i=1}^{n} (\boldsymbol{I}_i \boldsymbol{\omega}_i + \boldsymbol{r}_i \times m_i \boldsymbol{v}_i) = \boldsymbol{C}_0 \tag{5}$$

where $\boldsymbol{I}_i$ is the inertia matrix of link i expressed in the inertial global frame for each of the n links, $\boldsymbol{v}_i$ its velocity vector, $\boldsymbol{\omega}_i$ its angular velocity vector and $\boldsymbol{r}_i$ the position of the centre of mass of link i relative to the global centre of mass. The constant $\boldsymbol{C}_0$ will be later taken as zero to simplify the derivation since it only impacts the magnitude of the velocities and not the general behaviour of the system.

For the sake of this demonstration, the mechanism is simplified to a n-links serial manipulator with n-1 revolute joints. Then the link velocity are obtained as:

$$\boldsymbol{v}_i = \boldsymbol{v}_{i-1} + \boldsymbol{\omega}_{i-1} \times \boldsymbol{r}_{ki-1} - \boldsymbol{\omega}_i \times \boldsymbol{r}_{ki} \tag{6}$$

where k is the joint between link i and $i-1$. Knowing that $\boldsymbol{\omega}_i = \boldsymbol{\omega}_{i-1} + \dot{\theta}_k \boldsymbol{e}_k$ and substituting in (5) so that $\boldsymbol{\omega}_1$ only depends on geometric parameters, joint inputs ($\dot{\theta}_j$,$\boldsymbol{e}_j$) and $\boldsymbol{v}_1$, we get:

$$\begin{aligned}\boldsymbol{\omega}_1 \sum_{i=1}^{n} \boldsymbol{I}_i + \sum_{j=1}^{k} \sum_{i=j+1}^{n} \boldsymbol{I}_i \dot{\theta}_j \boldsymbol{e}_j + \sum_{i=1}^{n} \boldsymbol{r}_i \times m_i \boldsymbol{v}_1 \\ + \sum_{i=2}^{n} \boldsymbol{r}_i \times m_i [\boldsymbol{\omega}_1 \times \boldsymbol{r}_{11} - (\boldsymbol{\omega}_1 + \dot{\theta}_1 \boldsymbol{e}_1) \times \boldsymbol{r}_{12}] \\ + \sum_{i=3}^{n} \boldsymbol{r}_i \times m_i [(\boldsymbol{\omega}_1 + \dot{\theta}_1 \boldsymbol{e}_1) \times \boldsymbol{r}_{22} - (\boldsymbol{\omega}_1 + \dot{\theta}_1 \boldsymbol{e}_1 + \dot{\theta}_2 \boldsymbol{e}_2) \times \boldsymbol{r}_{23}] \\ + \ldots\end{aligned}$$

where $\dot{\theta}_j$ is the angular velocity of joint j, $\boldsymbol{e}_j$ its direction and r_{12} is the position of joint 1 from the centre of link 2. The velocity of link 1 can be obtained directly from the conservation of the linear momentum (equation 4) and the velocities relation (6).

This equation needs to be expressed in the global inertial frame, so the rotation matrix of the first link is $\boldsymbol{Q}_{01} = \boldsymbol{R}_x(\phi)\boldsymbol{R}_y(\theta)\boldsymbol{R}_z(\psi)$, and each rotation matrix representing the rotation of link $i-1$ to link i follows the orientation of the corresponding joint as for instance: $\boldsymbol{Q}_{12} = \boldsymbol{R}_z(\alpha)$ for $e_k = [0,0,1]'$.

Equation (6) can be re-written as:

$$\boldsymbol{A}\boldsymbol{\omega}_1 = \boldsymbol{b}\dot{\theta} \tag{7}$$

hence we get a matrix equation to either determine the joint velocities from the desired orientation or the converse. For instance, for a 2-link one-joint system, we get the expression:

$$\boldsymbol{A} = I_1 + I_2 + m_1[(\boldsymbol{r}_{11} - \boldsymbol{r}_{12})\boldsymbol{r}_1^T - \boldsymbol{r}_1^T(\boldsymbol{r}_{11} - \boldsymbol{r}_{12})\boldsymbol{1}] \tag{8}$$

and

$$\boldsymbol{b} = -(I_2 \boldsymbol{e}_1 + m_1[\boldsymbol{r}_1 \times (\boldsymbol{e}_1 \times \boldsymbol{r}_{12})]) \tag{9}$$

Similar expressions were found for a general case and derived by Papadopoulos and Dubowsky in [32].

Using XYZ Euler angles (for compatibility with most simulation and CAD softwares) the relation between the angular velocity of the first body and the time derivatives of the Euler angles is:

$$\boldsymbol{\omega}_1 = \boldsymbol{Q}_{\omega\dot{\eta}} \dot{\boldsymbol{\eta}} \,, \tag{10}$$

where $\dot{\boldsymbol{\eta}} = \begin{bmatrix}\dot{\phi} & \dot{\theta} & \dot{\psi}\end{bmatrix}'$ and $\boldsymbol{Q}_{\omega\dot{\eta}} = \begin{bmatrix}\boldsymbol{e}_x & \boldsymbol{R}_x\boldsymbol{e}_y & \boldsymbol{R}_x\boldsymbol{R}_y\boldsymbol{e}_z\end{bmatrix}$.

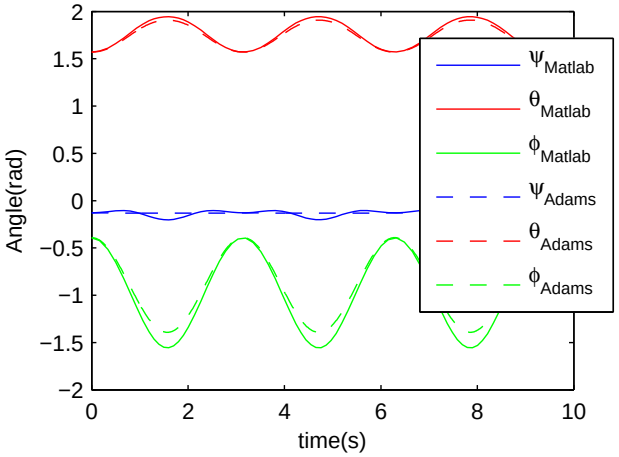

Figure 12: Simulation results comparison for $\dot{\theta} = 2sin(2t)$

In the context of a planar mechanism, we have direct control over only one of the three orientation angles, regardless of the number of links. The inverse system (getting joint velocity from desired orientation) is then overconstrained (more equations than unknowns).

4.2 Simulations

Simulations were conducted with a simplified 2-link one-revolute-joint Matlab model and compared to the results for an identical geometry and dynamics in MSC Adams. The results show that our equations correctly represent the behaviour of such a mechanism, but that some care should be

taken with the integration solver used. For simulation times longer than 40 to 50 seconds, we begin to observe a drift with a simple Euler integration as well as with the c++ MSC Adams solver. Using a robust medium-order Matlab solver (*ode*45) the precision over larger simulation times remains good.

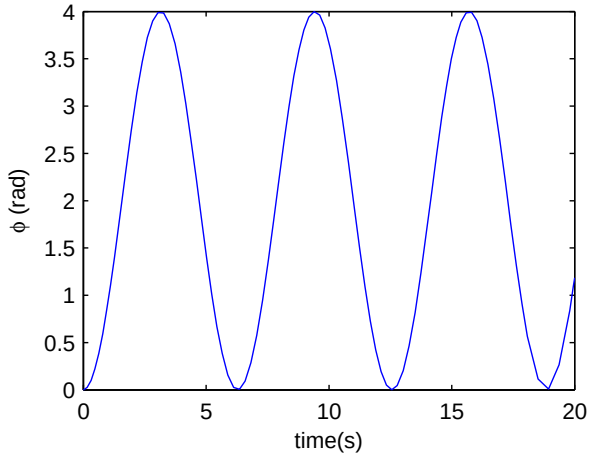

Figure 13: Desired orientation trajectory for 2-link one-revolute-joint mechanism ($\psi = \theta = 0$)

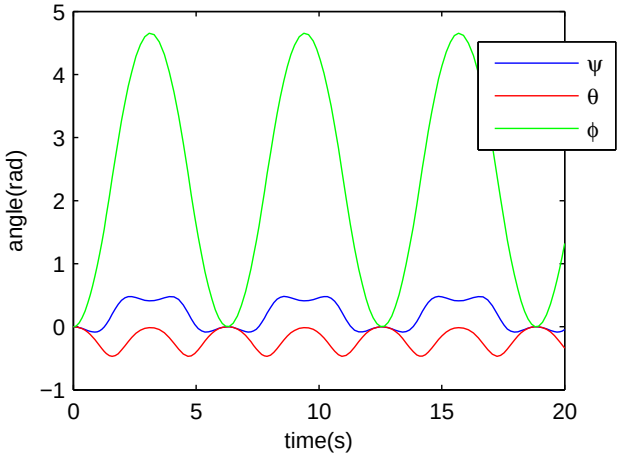

Figure 14: Resulting trajectory for 2-link one-revolute-joint mechanism

Figure 12 compares the results where $\dot{\theta}$ in equation (7) is imposed and $\boldsymbol{\omega}_1$ is determined by inverting matrix $\boldsymbol{A}$. Now a more pratical derivation is to impose a movement of the first link ($\boldsymbol{\omega}_1$ or the Euler angles) and find the required joint movement. This system has only one actuated joint for three desired orientational degrees of freedom and the least-squares solution is therefore computed, namely:

$$\dot{\theta} = (\boldsymbol{b}'\boldsymbol{b})^{-1}\boldsymbol{b}'(\boldsymbol{A}\boldsymbol{\omega}_1) \tag{11}$$

Using the same mass for both links ($m_{1,2} = 20kg$), same length ($L_{1,2} = 0.25m$) and the following inertia matrices, we obtain the results shown in figures 13 and 14:

$$I_1 = \begin{bmatrix} 40 & 0 & 20 \\ 0 & 40 & 20 \\ 20 & 20 & 40 \end{bmatrix}, I_2 = \begin{bmatrix} 40 & 0 & 0 \\ 0 & 40 & 0 \\ 0 & 0 & 40 \end{bmatrix} \tag{12}$$

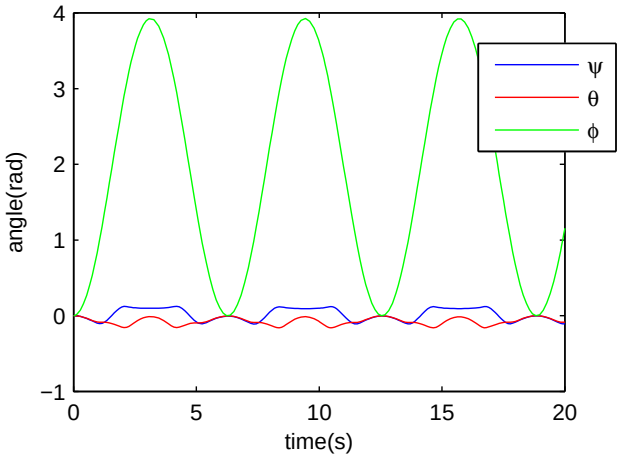

Figure 15: Resulting trajectory for 3-links 2-revolute-joints (Adapted geometry design - EQ.12)

Adding another body to the free end of the second, through a new revolute joint not parallel to the previous, leads to a system with better control of its orientation as seen in figure 15. For this simulation the same desired trajectory as in figure 13 was used and the least-squares solution for the joints velocities is computed. The third link is identical to the second one (diagonal inertial matrix).

The physical parameters of the links have a great impact on the re-orientation performances. For instance, using these inertia matrices instead:

$$I_1 = \begin{bmatrix} 40 & 30 & 30 \\ 30 & 40 & 30 \\ 30 & 30 & 40 \end{bmatrix}, I_2 = 2I_1, I_3 = I_1 \tag{13}$$

with $m_1 = 20kg$, $m_2 = 2m_1$ and $m_3 = m_1$, leads to a resulting trajectory that is less acurate, as shown in figure 16.

By extrapolation of the difference between figures 15 and 16 we conclude that the geometric properties of the mechanism can be set in such a way that better control is achieved.

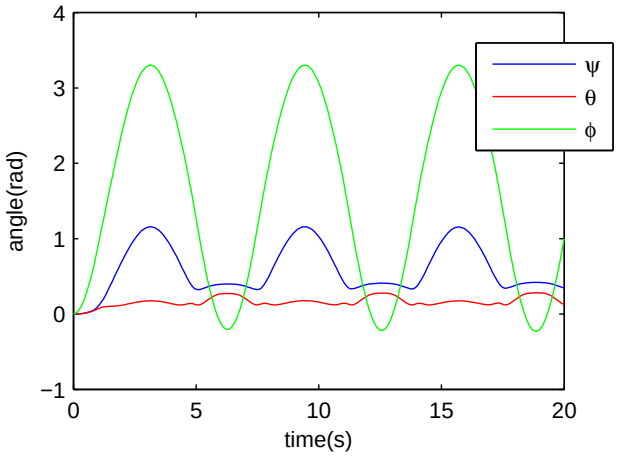

Figure 16: Resulting trajectory for 3-links 2-revolute-joint (Less acurate geometry design - EQ.13)

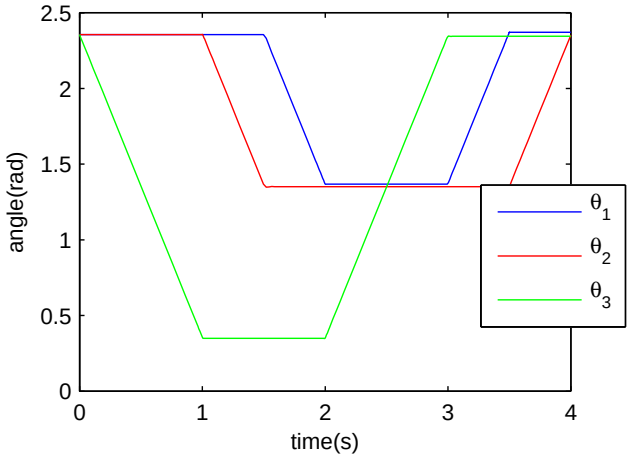

Figure 18: Input joint angles for 9-link 9-revolute-joint mechanism (triangular unit)

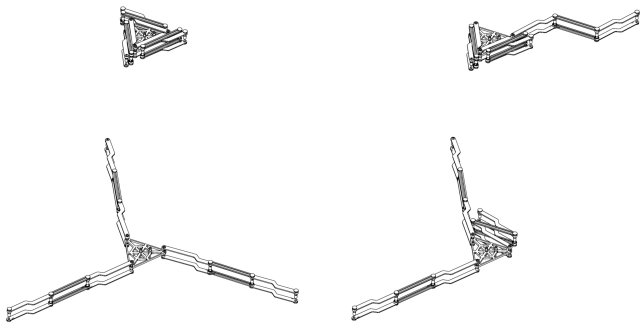

Figure 17: Simulation steps of mechanism re-orientation example

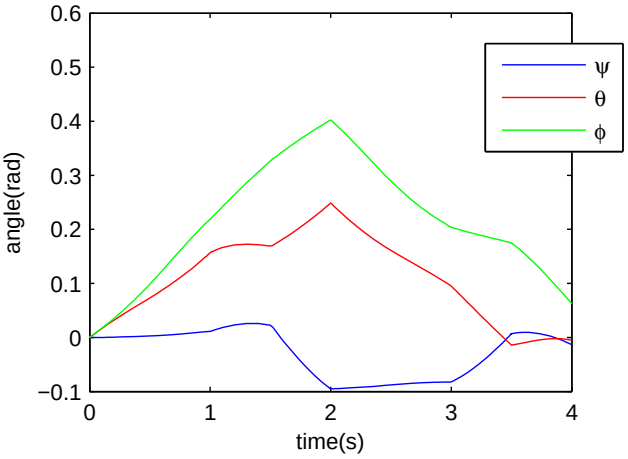

Figure 19: Resulting trajectory for 9-link 9-revolute-joint mechanism (triangular unit)

It should then be feasible to use such results in the mechanism design process.

A complete triangular face unit with 3 links per leg and 3 legs based on the mechanism of the previous section is then simulated as shown in figure 17.

The trajectory resulting from the asymmetrical input trajectory of figure 18 is shown in figure 19. Each leg is actuated separately and thus influences the final orientation of the device by moving through configurations of different inertia. In figure 18, the first leg is extended while the other two are retracted. The first leg then retracts itself when leg 2 and 3 are all extended. The effect is a final mechanism configuration identical to the intial state but whose orientation has changed.

5 CONCLUSION

We presented a new mechanism and mechanism concept that can be used to design a net or membrane device to capture or slow down the small-to-medium sized debris in LEO.

Another closely related application is to use the mechanism as an end of life device to enhance the drag of a spacecraft when its lifetime expired. For instance the area of the satellite EnviSat is $260m^2$, equipped with a $0.15km^2$ slow-down device, it would greatly enhance the drag force. For de-orbiting systems, the idea is to reach a low ballistic coef-

ficient, i.e. the ratio between the mass and the area, times the drag coefficient; the lower this index, the slower the spacecraft will move when starting its re-entry sequence. The most common strategy for de-orbiting spacecraft is to use thrusters, but then limit the lifetime of the device due to its limited fuel ressources. A light and compact device such as the mechanism presented in this paper could be a good solution.

Future works are to be conducted in using the internal actuators of the deployable system for re-orientation to determine design strategies of a mechanism optimizing its orientation control. It is also planned to extend this approach to other kinds of deployable structures.

6 ACKNOWLEDGEMENT

The authors would like to acknowledge the financial support of the Natural Sciences and Engineering Research Council of Canada (NSERC) and the Canada Research Chair Program.

References

[1] J.-C. Liou, A note on active debris removal, Orbital Debris - Quarterly News 15 i3 (july 2011) 4–5.

[2] W. A. Imbriale, S. S. Gao, L. Boccia, Space Antenna Handbook, Wiley, USA, 2012.

[3] D. Kessler, B. Cour-Palais, Collision frequency of artificial satellites: the creation of debris belt., Journal of geophysical research (1978) 2637–2646.

[4] C.Bonnal, J.-M. Ruault, M.-C. Desjean, Active debris removal: Recent progress and current trends, Acta Astronautica 85 (2013) 51–60.

[5] T. Kelso, Iridium 33/cosmos 2251 collision, Tech. rep., CelesTrack, [from website; accessed 11-April-2013] (2009).

[6] Orbital debris - a technical assessment, Tech. rep., National Academy press (1995).

[7] J. Liou, N. Johnson, N. Hill, Controlling the growth of future leo debris population with active debris removal., Acta Astonautica 66 (2010) 648–653.

[8] J. Liou, An active debris removal parametric study for leo environment remediation., Advance in space research 47 (2011) 1865–1876.

[9] N. L. Johnson, The world state of orbital debris measurements and modeling, Acta Astronautica 54 (2004) 267–272.

[10] A. Moussi, G. Drolshagen, J. McDonnell, J. Mandeville, A. Kearsley, H. Ludwig, Hypervelocity impacts on hst solar arrays and the debris and meteoroids population, Advances in Space Research 35 (2005) 1243–1253.

[11] G. Graham, A. Kearsley, G. Drolshagen, N. McBride, S. Green, I. Wright, Microparticule impacts upon hst solar cells, Advances in Space Research 28 (2001) 1341–1346.

[12] F. Horz, G. Cress, M. Zolensky, T. See, R. Bernhard, J. Warren, Optical analysis of impact features in aerogel from the orbital debris collection experiment on the mir station, Tech. Rep. NASA/TM-1999-209372, NASA Johnson Space Center (1999).

[13] K. Ramohalli, Economical in situ processing for orbital debris removal., Acta Astonautica 26 (1992) 55–60.

[14] N. L. Johnson, E. Stansbery, J.-C. Liou, M. Horstman, C. Stokely, D. Whitlock, The characteristics and consequences of the break-up of the fengyun-1c spacecraft, Acta Astronautica 63 (2008) 128–135.

[15] Dow Corning, Dow Corning 93 500 - Space Grade Encapsulant, [from website; accessed 11-April-2013].

[16] NASA, Launch propulsion system roadmap, Technology Area 01. (2010).

[17] Arianespace Service & Solutions, Ariane 5 User's Manual (2011).

[18] S. Pellegrino, Deployable Structures, Springer-Verlag Wien, New-York, 2001.

[19] S. Group, W. G. 4, Iadc space debris mitigation guidelines, Tech. rep., Inter-agency Space Debris Coordination Committee (2007).

[20] V. Carandente, GennaroZuppardi, RaffaeleSavino, Aerothermodynamic and stability analyses of a deployable re-entry capsule, Acta Astronautica 93 (2013) 291–303.

[21] C. Gosselin, D. Gagnon-Lachance, Expandable polyhedral mechanisms based on polygonal one-degree-of-freedom faces, Proceedings of Institution of Mechanical Engineers, Part C: Journal of Mechanical Engineering Science 220 (2006) 1011.

[22] K. Wohlhart, Cupola linkages, Proceedings of the 12th IFToMM World Congress (2007) 319–324.

[23] G. Wei, J. S. Dai, Synthesis of a family of regular deployable polyhedral mechanisms (dmps), Latest advances in robot kinematics (2012) 123–130.

[24] D. St-Onge, C. Gosselin, Synthesis and design of one-degree-of-freedom planar deployable mechanism with a large expansion ratio, Tech. rep., Laval University (2014).

[25] S. Britvec, Stability and Optimization of flexible space structures, Birkhauser, Basel, Germany, 1995.

[26] S. Nishida, T. Yoshikawa, Space debris capture by a joint compliance controlled robot, Proceedings of the 2003 IEEE/ASME Inter. Conf. on Advanced Intelligent Mechatronics (2003) 496 – 502.

[27] H. Gui, L. Jin, S. Xu, Attitude maneuver control of a two-wheeled spacecraft with bounded wheel speed, Acta Astronautica 88 (2013) 98–107.

[28] B. Celerier, Propulsion system for controlling the orbit and controlling the attitude of a satellite (Nov. 2013).

[29] E. Silani, M. Lovera, Magnetic spacecraft attitude control: a survey and some new results, Control Engineering Practice 13 (2005) 357–371.

[30] M. Shibli, Unified modeling approach of kinematics, dynamics and control of a free-flying space robot interacting with a target satellite, Intelligent Control and Automation 2 (2011) 8–23.

[31] Y.-L. Kuoa, T.-L. Wu, Open-loop and closed-loop attitude dynamics and controls of miniature spacecraft using pseudowheels, Computers and Mathematics with Applications 64 (2012) 1282–1290.

[32] S. Dubowsky, E. Papadopoulos, The kinematics, dynamics, and control of free-flying and free-floating space robotic systems, IEEE Transactions on robotics and automation 9 (1993) 531.

[33] I. Kolmanovsky, N. H. McClamroch, V. T. Coppola, New results on control of multibody systems which conserve angular momentum, Journal of dynamical and control systems 1 (1995) 447–462.

[34] N. Shiroma, H. Arai, K. Tanie, Nonholonomic motion planning for coupled planar rigid bodies with passive revolute joints, Int. journal of Robotics Research 21 (2002) 563.

[35] N. Sreenath, Nonlinear control of planar multibody systems in shape space, Mathematics of Control, Signals and Systems 5 (1992) 343–363.

[36] M. Reyhanoglu, N. H. McClamroch, Planar reorientation maneuvers of space multibody systems using internal controls, Journal of guidance, control and dynamics 15 (1992) 1475.

[37] M. Reyhanoglu, N. H. McClamroch, Reorientation of space multibody systems maintaining zero angular momentum, Proceedings of Navigation and Control Conference 1 (1991) 1330.

[38] I. V. Kolinanovsky, N. H. McClamroch, V. T. Coppola, Exact tracking for a planar multilink in space using internal actuation, Proc. of the American Control Conference (1994) 10–20.

[39] J. Shen, Nonlinear control of multibody systems with symmetries via shape change, Ph.D. thesis, University of Michigan (2002).